AIMS Mathematics, 11(4): 8966–8987.
DOI: 10.3934/math.2026370
Received: 31 January 2026
Revised: 09 March 2026
Accepted: 18 March 2026
Published: 02 April 2026

https://www.aimspress.com/journal/Math

*Research article*

# A robust dual spectral-spline framework for stochastic fractional equations perturbed by white noise

**Aisha F. Fareed[1,2,*], Mourad S. Semary[2,3], Dokhyl M. Alqahtani[1], Emad A. Mohamed[1] and Ahmed G. Khattab[2]**

[1] Department of Electrical Engineering, College of Engineering, Prince Sattam bin Abdulaziz University, Al Kharj 16278, Saudi Arabia
[2] Basic Engineering Sciences Department, Benha Faculty of Engineering, Benha University, Benha 13512, Egypt
[3] Basic Sciences Department, Faculty of Engineering, Badr University in Cairo BUC, Cairo 11829, Egypt

* **Correspondence:** Email: a.fareed@psau.edu.sa.

**Abstract:** In this research, we introduced dual numerical frameworks for stochastic time-fractional partial differential equations (STFPDEs) driven by additive white noise. The sifted Vieta-Fibonacci polynomials (SVFPs) and the ten non-polynomial cubic spline (TNPCS) approach are the foundation for our spectral-spline frameworks. The suggested methods were used to solve two STFPDEs: The nonlinear STF Burger's equation and the linear STF heat equation, and they approximated stochastic trajectories with high precision. This analysis showed a substantial decrease in variance, and the mean profile remained constant despite stochastic effects. The key contribution of this paper is the introduction of two separate spectral-spline numerical approaches derived from the SVFPs and the TNPCS formulations for handling stochastic fractional models. By applying each approach independently and comparing their results side by side, the study provides clearer insight into their numerical performance, stability, and practical usefulness in simulating stochastic fractional dynamics. All computations were implemented using *Mathematica 12* and *Jupyter Notebook*, which ensured the validity, dependability, and reliability of our algorithms against noise propagation.

**Keywords:** white noise; Burger's equation; heat equation; orthogonal polynomials; Vieta-Fibonacci polynomials; stochastic differential equations
**Mathematics Subject Classification:** 60H15, 65C30, 65N35

## 1. Introduction

Fractional calculus uses the basic notions of differentiation and integration and goes much further with them. Instead of sticking with integer steps, it works with operators of any order, even real or complex numbers. It gives us a smooth, continuous range for analyzing problems, where you can go for half-derivatives or anything in between. In the late $17^{th}$ century, renowned mathematicians such as Leibniz, Euler, and Liouville established its theoretical foundations. In recent decades, fractional calculus has found its place in the real world for modeling many complex systems, especially where we have memory effects, non-local interactions, or long-range dependencies [1–3].

Time-fractional partial differential equations (TFPDEs) sit at the heart of this shift. Instead of using the standard time derivatives, they bring in fractional operators defined in the sense of Riemann-Liouville or Caputo. These TFPDEs do not capture only the current occurrences in a system, as they reach back and fold in the entire history. This non-local memory makes them incredibly useful across many fields, like anomalous diffusion, relaxation oscillations, long-range correlations, or spatial heterogeneity [4–6].

Since deterministic models do not include intrinsic fluctuations or noises within the surrounding environment, these fluctuations are contained naturally within the progress of the respective physical process. The inclusion of stochastic processes, in the form of additive white noise, leads to the development of stochastic TFPDEs. It results in the formation of a complete and meticulous framework of mathematics that can possibly handle the inherent memory and randomness of the environment.

Due to the growing attention in stochastic fractional models, obtaining reliable numerical approximations for such systems remains a challenging task. The simultaneous presence of fractional memory effects and stochastic perturbations often leads to significant computational complexity and stability issues for many traditional numerical schemes. In addition, several available techniques may require much computational effort or may suffer from reduced accuracy when stochastic noise propagates through the system. These challenges motivate the search for efficient numerical frameworks that can capture the fractional dynamics and the stochastic behavior in a stable and accurate manner.

The literature indicates the existence of a varied spectrum of analysis and computation strategies that have been established to solve the problem of stochastic partial differential equations (SPDEs) and their fractional versions (stochastic time-fractional partial differential equations (STFPDEs)). For instance, the stochastic version of the Simpson method [7] and the fractional integral transform method following the application of the homotopy perturbation method [8] have been highlighted to exhibit satisfactory potential on the solutions of the problem of interest. Other prevalent methods include the application of the spectral and polynomial-based techniques following the operational method of Legendre polynomials [9], spectral stochastic methods [10], shifted Vieta-Fibonacci polynomials (SVFPs) [11], the ten non-polynomial cubic spline (TNPCS) technique [12], and the finite element method along with the Tau-finite difference method [13,14], the fast discrete Fourier transform method [15], the Galerkin collocation hybrid method [16], the conformable fractional Temimi–Ansari method [17,18], and the stochastic exponential method [19].

Upon the foundational framework that was given in [11], we make a substantial advancement in the state-of-the-art in that it generalizes the methodology to the realm of stochastic fractional domains. Rigorous frameworks in terms of numerical approximation of the stochastic dynamics of TFPDEs subject to additive white noise perturbations are devised. In this research, the novelty of our work lies in extending and employing two distinct spectral-spline-based numerical strategies for stochastic time-fractional models driven by additive white noise. Unlike several approaches that focus on deterministic

fractional equations, we investigate the performance of SVFP-based spectral approximation and the TNPCS spline formulation within a stochastic fractional setting. The two techniques are implemented independently, and their numerical behavior is carefully compared to evaluate their accuracy, robustness, and computational suitability for stochastic fractional dynamics.

The added value of this study is twofold. First, it provides reliable numerical frameworks capable of approximating stochastic fractional dynamics while maintaining stable mean behavior under noise perturbations. Second, the comparative investigation of the two approaches offers useful insight into their practical performance, which may assist researchers in selecting appropriate numerical tools for similar stochastic fractional problems arising in physics, engineering, and applied sciences.

The proposed frameworks are applied to two benchmark models: STF Burger's equation (STFBE) [20]:

$$\mathcal{U}_{xx} = D_t^{\alpha}\mathcal{U} + \mathcal{U}\mathcal{U}_x + \sigma\mathcal{U}n(t),\ (x,t) \in \mathfrak{V}, \tag{1.1}$$

and STF heat equation (STFHE) [22]:

$$\mathrm{D}_{\mathrm{t}}^{\alpha}\mathcal{U} = \varepsilon\mathcal{U}_{\mathrm{xx}} + \sigma\mathcal{U}n(\mathrm{t}) = 0,\ (\mathrm{x},\mathrm{t}) \in \mathfrak{V}, \tag{1.2}$$

where $\mathfrak{V} = [a,b] \times [0,T]$, $\rho$, $\varepsilon$, and $\sigma$ are arbitrary constants, and $D_t^{\alpha}\mathcal{U}$ is the Caputo-fractional derivative of order $\alpha$ defined as:

$$D_t^{\alpha C}\mathcal{U}(x,t) = \frac{1}{\Gamma(1-\alpha)}\int_0^t \frac{\partial\mathcal{U}(x,\xi)}{\partial\xi}(t-\xi)^{-\alpha}\,d\xi,\ 0 < \alpha < 1. \tag{1.3}$$

The fractional operator $D_t^{\alpha C}$ has the following properties:

- $D_t^{\alpha C}(\gamma) = 0$, where $\gamma$ is a constant,
- $D_t^{\alpha C}(t^n) = \begin{cases} \frac{\Gamma(n+1)}{\Gamma(n-\alpha+1)}t^{n-\alpha}, & n > 0, \\ 0, & otherwise. \end{cases}$

These STFPDEs have incorporated the white noise term, expressed as $n(t) = \varsigma\frac{d}{dt}\mathcal{B}(t)$, where $\mathcal{B}(t)$ denotes the Brownian motion process, and it is also characterized by properties such as zero expectation and variance, expressed as $\varsigma^2$. These equations may be unified and expressed in the form of a comprehensive generalized equation, and it may be expressed as follows:

$$\varepsilon\mathcal{U}_{xx} = D_t^{\alpha}\mathcal{U} + \rho\mathcal{U}\mathcal{U}_x + \sigma\mathcal{U}n(t),\ (x,t) \in \mathfrak{V},\ 0 < \alpha < 1. \tag{1.4}$$

This general structure enables us to construct specific physical models, depending on the value of the $\rho$ parameter:

- STF Burger's equation: Set $\rho = 1$, we get Eq (1.1).
- STF heat equation: Set $\rho = 0$, we obtain Eq (1.2).

Each numerical approach considered in this research presents particular advantages and certain limitations. The SVFP-based spectral approach benefits from its strong approximation capability and rapid convergence when representing smooth solution profiles. On the other hand, the TNPCS formulation provides flexibility and stability in the numerical treatment of differential operators through spline-based interpolation. However, as with many spectral and spline techniques, the overall performance may depend on parameter selection and discretization settings. Investigating these aspects

through numerical experiments enables us to better understand the practical strengths and limitations of both approaches.

This paper is structured as follows. In Section 2, we present the mathematical preliminaries of SVFPs and TNPCS schemes. In Section 3, we introduce the description of the schemes numerically, which are designed and developed by focusing on the nuances of the STFBE and the STFHE models. In Section 4, we present the numerical experiments and their validations, including the error analysis of the scheme in relation to the other methods in the literature. In the last section, Section 5, we present the concluding remarks and discuss the broader implications of this work.

## 2. Theoretical foundations in stochastic domains

In this section, we establish the theoretical framework for the SVFPs. These polynomials have two purposes: To act as a spatial basis within stochastic domains and as a temporal basis within stochastic fractional domains. Furthermore, we provide the core formulation of the TNPCS method adapted for applications in fractional domains.

### *2.1. SVFPs in stochastic domains*

Consider $\mathcal{V}_\ell(x)$ as the VFPs, which are defined over $x \in [-2, 2]$ as follows:

$$\mathcal{V}_\ell(x) = \frac{\sin(\ell\theta)}{\sin(\theta)}, \tag{2.1}$$

where $\theta = \cos^{-1}\left(x/2\right) \in [0, \pi]$, and $\ell = 0, 1, 2, \ldots, M_x$. Their recurrence relation is: $\mathcal{V}_0(\mathrm{x}) = 0$, $\mathcal{V}_1(\mathrm{x}) = 1$, and

$$\mathcal{V}_\ell(\mathrm{x}) = \mathrm{x}\mathcal{V}_{\ell-1}(\mathrm{x}) - \mathcal{V}_{\ell-2}(\mathrm{x}), \ \ell \geq 2, \tag{2.2}$$

Additionally, their orthogonality condition with the weight function $\omega(x) = \sqrt{4 - x^2}$ is defined as:

$$\langle \mathcal{V}_\ell(x), \mathcal{V}_m(x) \rangle_\omega = \int_{-2}^{2} \mathcal{V}_\ell(x)\mathcal{V}_m(x)\omega(x)dx = (2\pi)\delta_{\ell m}. \tag{2.3}$$

In recent literature, VFPs have been extensively applied to solve a wide range of complex differential models. As demonstrated in [22–24], these polynomials provide a robust framework for basic fractional diffusion and integro-differential systems. Furthermore, the specialized methodologies developed in [25,26] illustrate the adaptability of VFPs to wavelet-based transformations and the resolution of equations involving weakly singular kernels. Finally, research in [27,28] highlights their effectiveness in constructing operational matrices for variable-order systems and high-order dispersive models, such as the fifth-order fractional KdV equation.

Assume that $\tilde{\mathcal{V}}_\ell(x)$ denotes the SVFPs in spatial domains over $x \in [a, b]$. Then, by applying a linear transformation: $\tilde{x} = \frac{2}{b-a}[2x - (a+b)]$ to Eq (2.2), the recurrence relation of SVFPs is: $\tilde{\mathcal{V}}_0(x) = 0$, $\tilde{\mathcal{V}}_1(x) = 1$, and

$$\tilde{\mathcal{V}}_\ell(x) = \frac{2}{b-a}[2x - (a+b)]\tilde{\mathcal{V}}_{\ell-1}(x) - \tilde{\mathcal{V}}_{\ell-2}(x), \ \ell \geq 2. \tag{2.4}$$

Additionally, their orthogonality requirement with the weight function $\tilde{\omega}(x) = \sqrt{(b-x)(x-a)}$ is given as:

$$\langle \tilde{\mathcal{V}}_\ell(x), \tilde{\mathcal{V}}_m(x) \rangle_{\tilde{\omega}} = \int_a^b \tilde{\mathcal{V}}_\ell(x)\tilde{\mathcal{V}}_m(x)\tilde{\omega}(x)\, dx = \frac{\pi}{8}(b-a)^2\delta_{\ell m}. \tag{2.5}$$

The spatial SVFPs function can be presented in matrix form as:

$$\tilde{\mathcal{V}}(x) = A.P(x), \tag{2.6}$$

where $A$ represents the coefficient matrix obtained from the recurrence relation (2.4) and

$$P(x) = [1, x, x^2, \dots, x^{M_x}]^T.$$

For $M_x = 4$, we get:

$$A = \begin{pmatrix} 1 & 0 & 0 & 0 & 0 \\ -2 & \frac{4}{b-a} & 0 & 0 & 0 \\ 3 & \frac{-16}{b-a} & \frac{16}{(b-a)^2} & 0 & 0 \\ -4 & \frac{40}{b-a} & \frac{-96}{(b-a)^2} & \frac{64}{(b-a)^3} & 0 \\ 5 & \frac{-80}{b-a} & \frac{336}{(b-a)^2} & \frac{-512}{(b-a)^3} & \frac{256}{(b-a)^4} \end{pmatrix}$$

and

$$P(x) = [1, x, x^2, x^3, x^4]^T.$$

The first-order derivative of spatial SVFPs is obtained in reduced matrix form as:

$$D^{(1)}\left(\tilde{\mathcal{V}}_\ell(x)\right) = \left(\tfrac{4}{b-a}\right) D^{(1)}_{m,\ell}.A.P(x), \tag{2.7}$$

where $\ell = 1{:}\,M_x,\ m = 0{:}\,M_x - 1$, and

$$D^{(1)}_{m,\ell} = \begin{cases} 0, & m = 0, \\ \ell, & m \neq 0 \wedge \ell \leq m \wedge (m-\ell) \text{ is even}, \\ 0, & \text{otherwise.} \end{cases}$$

The $n^{\text{th}}$-order derivative of spatial SVFPs is represented as:

$$D^{(n)}\left(\tilde{\mathcal{V}}_\ell(x)\right) = \left(D^{(1)}\right)^n\left(\tilde{\mathcal{V}}_\ell(x)\right) = \left(\tfrac{4}{b-a}\right)^n \left(\underbrace{D^{(1)}_{m,\ell} \times D^{(1)}_{m,\ell} \times \dots \times D^{(1)}_{m,\ell}}_{n-\text{times}}\right).A.P(x). \tag{2.8}$$

*2.2. SVFPs in stochastic fractional domains*

Let $\tilde{\mathcal{F}}_\ell(t)$ denote the SVFPs in temporal domains over $t \in [0, T]$. Then, by applying a linear transformation, $\tilde{t} = \frac{4}{T}t - 2$, to Eq (2.2), the recurrence relation of SVFPs is given as:

$$\tilde{\mathcal{F}}_0(t) = 0,\ \tilde{\mathcal{F}}_1(t) = 1,$$

and

$$\tilde{\mathcal{F}}_\ell(t) = \left[\tfrac{4}{T}t - 2\right]\tilde{\mathcal{F}}_{\ell-1}(t) - \tilde{\mathcal{F}}_{\ell-2}(t),\ \ell \geq 2, \tag{2.9}$$

Additionally, their orthogonality condition with $\tilde{\omega}(t) = \sqrt{t(T-t)}$ is defined as:

$$\langle \tilde{\mathcal{F}}_\ell(t), \tilde{\mathcal{F}}_n(t) \rangle_{\tilde{\omega}} = \int_0^T \tilde{\mathcal{F}}_\ell(t)\tilde{\mathcal{F}}_n(t)\tilde{\omega}(t)dt = \frac{\pi}{8}T^2\delta_{\ell n}. \tag{2.10}$$

The temporal SVFPs function in matrix form:

$$\tilde{\mathcal{F}}(t) = B.Q(t), \tag{2.11}$$

where $B$ represents the coefficient matrix obtained from the recurrence relation (2.9) and

$$Q(t) = [1, t, t^2, \dots, t^{M_t}]^T.$$

For $M_t = 4$, we get:

$$B = \begin{pmatrix} 1 & 0 & 0 & 0 & 0 \\ -2 & 4T^{-1} & 0 & 0 & 0 \\ 3 & -16T^{-1} & 16T^{-2} & 0 & 0 \\ -4 & 40T^{-1} & -96T^{-2} & 64T^{-3} & 0 \\ 5 & -80T^{-1} & 336T^{-2} & -512T^{-3} & 256T^{-4} \end{pmatrix},$$

and

$$Q(t) = [1, t, t^2, t^3, t^4]^T.$$

The first-order fractional derivative of temporal SVFPs is given as:

$$D_t^{\alpha C}\tilde{\mathcal{F}}_\ell(t) = \frac{4}{T}D_t^{\alpha C}\tilde{\mathcal{F}}(t) = \frac{4}{T}D_t^{\alpha C}.B.Q(t) = \frac{4}{T}B.[D_t^{\alpha C}Q(t)], \tag{2.12}$$

Applying Caputo's fractional derivative to Eq (2.12), we get

$$D_t^{\alpha C}Q(t) = D_t^{\alpha C}[1, t, t^2, \dots, t^{M_t}]^T = \left[0, \frac{\Gamma(2)}{\Gamma(2-\alpha)}t^{1-\alpha}, \frac{\Gamma(3)}{\Gamma(3-\alpha)}t^{2-\alpha}, \dots, \frac{\Gamma(M_t+1)}{\Gamma(M_t+1-\alpha)}t^{M_t-\alpha}\right]^T = \Lambda_\alpha(t).Q(t),$$

Hence,

$$D_t^{\alpha C}\tilde{\mathcal{F}}_\ell(t) = \frac{4}{T}B.\Lambda_\alpha(t).Q(t), \tag{2.13}$$

where $\Lambda_\alpha(t) = \left[0, \frac{\Gamma(2)}{\Gamma(2-\alpha)}t^{-\alpha}, \frac{\Gamma(3)}{\Gamma(3-\alpha)}t^{-\alpha}, \dots, \frac{\Gamma(M_t+1)}{\Gamma(M_t+1-\alpha)}t^{-\alpha}\right]^T$.

### *2.3. TNPCS method in stochastic fractional domains*

The TNPCS function $S_i(x,t)$ is defined as in [29]:

$$S_i(x,t_j) = a_{ij}\left(k_1e^{\lambda_1\tau(x-x_i)} + k_2e^{-\lambda_1\tau(x-x_i)}\right) + b_{ij}\left(k_3e^{\lambda_2\tau(x-x_i)} + k_4e^{-\lambda_2\tau(x-x_i)}\right) + c_{ij}(x-x_i) + d_{ij}, \tag{2.14}$$

for $x_i \le x \le x_{i+1}$ and $i = 0, 1, 2, \dots, M_x$, where $\tau, \lambda_1, \lambda_2, k_1, k_2, k_3$, and $k_4$ are constants that can be assumed to get the required forms of the TNPCS functions, as given in Table 1 in [12,29]. The spline coefficients $a_{ij}, b_{ij}, c_{ij}$, and $d_{ij}$ are discussed in detail in [29].

For $x \in [a,b]$, suppose that $x_i = a + ih$ with $M_x$ subintervals, $h = \frac{b-a}{M_x}$ and $i = 0{:}\,M_x$. For $t \in [0,T]$, assume $t_j = jk$, $j = 0{:}\,T$, and $k$ is the time step. By applying the continuity of the first derivative of the spline function, we establish that $S'_{i-1}(x_i,t_j) = S'_i(x_i,t_j)$. Hence,

$$\beta_0[\mathcal{U}_{xx}]_{i-1}^j + \beta_1[\mathcal{U}_{xx}]_i^j + \beta_2[\mathcal{U}_{xx}]_{i+1}^j = \frac{1}{h^2}\left(\mathcal{U}_{i-1}^j - 2\mathcal{U}_i^j + \mathcal{U}_{i+1}^j\right), \text{ for } i = 1,2,3, \dots, M_x - 1, \tag{2.15}$$

where $\beta_0$, $\beta_1$, and $\beta_2$ are some constants that need to be obtained by applying Taylor's expansion about $x_i$ to Eq (2.15). Then, the local truncation error $(T_i)$ is defined as:

$$T_i = (-1+\beta_0+\beta_1+\beta_2)[\mathcal{U}_{xx}]_i^j + h(-\beta_0+\beta_2)[\mathcal{U}_{xxx}]_i^j + \frac{h^2}{12}(-1+6\beta_0+6\beta_2)[\mathcal{U}_{xxxx}]_i^j$$
$$+\frac{h^3}{6}(-\beta_0+\beta_2)[\mathcal{U}_{xxxxx}]_i^j + O(h^4). \quad (2.16)$$

Assume $e_1 = -1+\beta_0+\beta_1+\beta_2$, $e_2 = -\beta_0+\beta_2$ and $e_3 = -1+6\beta_0+6\beta_2$, then for $e_1 = e_2 = e_3 = 0$, we obtain $\beta_0 = \beta_2 = \frac{1}{12}$, $\beta_1 = \frac{5}{6}$.

Thus, Eq (2.15) can be written as follows:

$$[\mathcal{U}_{xx}]_{i-1}^j + 10[\mathcal{U}_{xx}]_i^j + [\mathcal{U}_{xx}]_{i+1}^j = \frac{12}{h^2}\left(\mathcal{U}_{i-1}^j - 2\mathcal{U}_i^j + \mathcal{U}_{i+1}^j\right), \text{ for } i = 1,2,3,\dots,M_x-1. \quad (2.17)$$

Substituting the second spatial derivatives with the left-hand side of Eq (2.17) transforms the governing equation into an algebraic equation system. Solving this system results in a numerical approximation of the target stochastic fractional model.

To evaluate the accuracy of the proposed TNPCS spatial discretization, the truncation error associated with the spline approximation is examined. Starting from the continuity condition of the first derivative and the relation given in Eq (2.15), Taylor series expansions about the grid point $x_i$ are used to obtain the truncation error expression presented in Eq (2.16).

The coefficients $\beta_0, \beta_1$, and $\beta_2$ determine the magnitude of the leading error terms. To improve the accuracy of the approximation, these parameters are selected so that the first three error coefficients vanish. Specifically, by imposing

$$e_1 = -1+\beta_0+\beta_1+\beta_2 = 0,$$
$$e_2 = -\beta_0+\beta_2 = 0,$$
$$e_3 = -1+6\beta_0+6\beta_2 = 0.$$

Substituting these values into Eq (2.15) yields the compact relation presented in Eq (2.17). With this choice, the lower-order error terms cancel, and the leading truncation term becomes proportional to $h^4$. Therefore, the TNPCS formulation provides a fourth-order accurate approximation for the second spatial derivative.

When the spatial discretization is combined with the temporal approximation used for the stochastic time-fractional derivative, the total numerical error depends on the spatial step $h$ and the time step $k$. Under the assumption that the exact solution is sufficiently smooth, the global error of the numerical approximation can be expressed in the general form

$$\left\|\mathcal{U}(x_i,t_i) - \mathcal{U}_i^j\right\| \le C(h^4+k^p),$$

where $C$ is a positive constant independent of the mesh parameters, and $p$ denotes the order of accuracy associated with the chosen time-fractional discretization.

This analysis confirms that the proposed TNPCS framework provides a high-order spatial approximation while maintaining stability and accuracy when applied to stochastic time-fractional models. The theoretical estimates are further supported by the numerical experiments presented in Section 4, where the computed results demonstrate good agreement with the expected convergence behavior.

## 3. Methodology: a spectral approach to stochastic heat and multi-dimensional stochastic Poisson equations

Based on the theoretical framework discussed, we present the numerical methodology adopted for solving stochastic TFPDEs. Two computational perspectives are considered, namely the spectral formulation based on SVFPs and the spline-based approximation using the TNPCS scheme.

### *3.1. Discretization of functions and noise via SVFPs*

Equations (2.6)–(2.8), (2.11), and (2.12) can be utilized to approximate the functions $\mathcal{U}(x,t,)$ and its derivatives using the SVFPs, as follows:

$$\mathcal{U}(x_i,t_j)=\left(\tilde{\mathcal{F}}(t_j)\otimes\tilde{\mathcal{V}}(x_i)\right)\mathcal{C}=\left[\left(B.Q(t_j)\right)\otimes\left(A.P(x_i)\right)\right]\mathcal{C}, \tag{3.1}$$

$$\frac{\partial^n}{\partial x^n}\mathcal{U}(x_i,t_j)=\left(\tilde{\mathcal{F}}(t_j)\otimes D^{(n)}\tilde{\mathcal{V}}(x_i)\right)\mathcal{C}=\left[\left(B.Q(t_j)\right)\otimes\left(\left(\frac{4}{b-a}\right)^n D^{(n)}.A.P(x_i)\right)\right]\mathcal{C}, \tag{3.2}$$

$$D_t^{\alpha C}\mathcal{U}(x_i,t_j)=\left(D_t^{\alpha C}\tilde{\mathcal{F}}(t_j)\otimes\tilde{\mathcal{V}}(x_i)\right)\mathcal{C}=\left[\left(\left(\frac{4}{T}\right)B.\Lambda_\alpha(t_j).Q(t_j)\right)\otimes\left(A.P(x_i)\right)\right]\mathcal{C}, \tag{3.3}$$

where $\mathcal{C}$ is the unknown coefficients, $\tilde{\mathcal{F}}(t_j)$ and $\tilde{\mathcal{V}}(x_i)$ are the SVFPs discussed in Section 2,

$$\mathcal{C}=\left[c_{1,1},c_{1,2},c_{1,3},\dots,c_{1,M_x+1},\dots,c_{M_t+1,1},\dots,c_{M_t+1,M_x+1}\right]^T,$$

$$\tilde{\mathcal{F}}(t_j)=\left[\tilde{\mathcal{F}}_1(t_j),\tilde{\mathcal{F}}_2(t_j),\tilde{\mathcal{F}}_3(t_j),\dots,\tilde{\mathcal{F}}_{M_t+1}(t_j)\right]^T,$$

$$\tilde{\mathcal{V}}(x_i)=\left[\tilde{\mathcal{V}}_1(x_i),\tilde{\mathcal{V}}_2(x_i),\tilde{\mathcal{V}}_3(x_i),\dots,\tilde{\mathcal{V}}_{M_x+1}(x_i)\right]^T,$$

and the symbol $\otimes$ represents the Kronecker-product of two matrices. If $\mathcal{X}_{i\times j}$ matrix and $\mathcal{Y}_{l\times m}$ matrix, then the Kronecker-product of $\mathcal{X}\otimes\mathcal{Y}$ is an $(il\times jm)$ matrix defined as:

$$\mathcal{X}\otimes\mathcal{Y}=\begin{bmatrix}x_{11}\mathcal{Y} & x_{12}\mathcal{Y} & \cdots & x_{1j}\mathcal{Y}\\ x_{21}\mathcal{Y} & x_{22}\mathcal{Y} & \cdots & x_{2j}\mathcal{Y}\\ \vdots & \vdots & \vdots & \vdots\\ x_{i1}\mathcal{Y} & x_{i2}\mathcal{Y} & \cdots & x_{ij}\mathcal{Y}\end{bmatrix}.$$

In the stochastic framework, the Brownian motion process $\mathcal{B}(t)$ and the white noise $n(t)$ are represented using a spectral expansion based on SVFPs. By projecting a stochastic process into a finite-dimensional space, the resultant distribution of $\mathcal{B}(t)$ is approximated by the SVFPs as follows:

$$\mathcal{B}(t_j)=\tilde{\mathcal{F}}(t_j)\Phi,\ \Phi=\left[\tilde{\mathcal{F}}(t_j)\right]^{-1}\mathcal{B}(t_j),j=0{:}M_t, \tag{3.4}$$

where $\Phi=\left[\varphi_1,\varphi_2,\varphi_3,\dots,\varphi_{M_{t+1}}\right]^T$ represents the unknowns and the values of $\mathcal{B}(t)$ at the nodes are generated using built-in stochastic functions within *Mathematica* software, and $\left[\tilde{\mathcal{F}}(t_j)\right]^{-1}$ denotes the pseudoinverse of $\tilde{\mathcal{F}}(t_j)$.

Since white noise is formally the derivative of Brownian motion, by utilizing the operational matrix of differentiation for SVFPs, we can express the white noise values at each level $j\geq 0$ as:

$$n(t_j)=\varsigma\circ D^{(1)}\tilde{\mathcal{F}}(t_j)\Phi\equiv\mathcal{N}_w. \tag{3.5}$$

*3.2. The spectral approach for STFPDEs*

To solve the STFPDEs numerically, we apply the SVFPs by substituting the previously defined expansions into the governing equation. By substituting the approximations for the unknown solution Eq (3.1), its derivatives Eqs (3.2) and (3.3), and the white-noise term Eq (3.5) into Eq (1.4), we evaluate the system at the collocation grid nodes $(x_i, t_j)$. The resulting discretized form is represented as:

$$\left[\left(\frac{4}{T}B.\Lambda_\alpha(t_j).Q(t_j)\right)\otimes\left(A.P(x_i)\right)\right]\mathcal{C}+\rho\left[\left(B.Q(t_j)\right)\otimes\left(A.P(x_i)\right)\right]\circ\left[\left(B.Q(t_j)\right)\otimes\left(\frac{4}{b-a}D^{(1)}_{m,i}.A.P(x_i)\right)\right]\mathcal{C}$$
$$-\varepsilon\left[\left(\left(B.Q(t_j)\right)\otimes\left(\left(\frac{4}{b-a}\right)^2D^{(2)}_{m,i}.A.P(x_i)\right)\right)\mathcal{C}\right]+\sigma(\mathcal{N}_w)\circ\left[\left(B.Q(t_j)\right)\otimes\left(A.P(x_i)\right)\right]\mathcal{C}=[\underline{\mathbf{0}}], \tag{3.6}$$

where $[\underline{\mathbf{0}}]$ represents a zero vector, and the symbol $\circ$ denotes the Hadamard product of two matrices.

Our process focuses on the interior grid points, where $j=1,2,3,\dots,M_t$ and $i=1,2,3,\dots,M_x-1$. By computing Eq (3.6) at these nodes, we construct the required system:

$$\left[\left(\left[\tilde{\mathcal{F}}^{(\alpha)}_t\right]^{(2:M_t+1)}\otimes\left[\tilde{\mathcal{V}}_x\right]^{(2:M_x+1)}\right)\mathcal{C}\right]+\rho\left[\left([\tilde{\mathcal{F}}_t]^{(2:M_t+1)}\otimes\left[\tilde{\mathcal{V}}_x\right]^{(2:M_x+1)}\right)\mathcal{C}\right]\circ\left[\left([\tilde{\mathcal{F}}_t]^{(2:M_t+1)}\otimes\left[\tilde{\mathcal{V}}^{(1)}_x\right]^{(2:M_x+1)}\right)\mathcal{C}\right]$$
$$-\varepsilon\left[\left([\tilde{\mathcal{F}}_t]^{(2:M_t+1)}\otimes\left[\tilde{\mathcal{V}}^{(2)}_x\right]^{(2:M_x+1)}\right)\mathcal{C}\right]+\sigma(\mathcal{N}_w)\circ\left[\left([\tilde{\mathcal{F}}_t]^{(2:M_t+1)}\otimes\left[\tilde{\mathcal{V}}_x\right]^{(2:M_x+1)}\right)\mathcal{C}\right]=[\underline{\mathbf{0}}], \tag{3.7}$$

where

$$\tilde{\mathcal{V}}_x=A.P(x_i),\ \tilde{\mathcal{V}}^{(1)}_x=\frac{4}{b-a}D^{(1)}_{m,i}.A.P(x),\ \tilde{\mathcal{V}}^{(2)}_x=\left(\frac{4}{b-a}\right)^2D^{(2)}_{m,i}.A.P(x),\ \tilde{\mathcal{F}}_t=B.Q(t_j),$$
$$\tilde{\mathcal{F}}^{(\alpha)}_t=\frac{4}{T}B.\Lambda_\alpha(t_j).Q(t_j),\ P(x_i)=[1,x_i,{x_i}^2,\dots,{x_i}^{M_x+1}],\ Q(t_j)=\left[1,t_j,{t_j}^2,\dots,{t_j}^{M_t+1}\right]^T,$$

$[\tilde{\mathcal{F}}_t]^{(2:M_t+1)}$ is a submatrix of rows $2:M_t+1$ and all columns of $\tilde{\mathcal{F}}_t$, $\left[\tilde{\mathcal{V}}_x\right]^{(2:M_x+1)}$ is a submatrix of rows $2:M_x$ and all columns of $\tilde{\mathcal{V}}_x$,

$$\tilde{\mathcal{F}}_t=\begin{bmatrix}\tilde{\mathcal{F}}_1(t_0) & \tilde{\mathcal{F}}_2(t_0) & \cdots & \tilde{\mathcal{F}}_{M_t}(t_0) & \tilde{\mathcal{F}}_{M_t+1}(t_0)\\ \tilde{\mathcal{F}}_1(t_1) & \tilde{\mathcal{F}}_2(t_1) & \cdots & \tilde{\mathcal{F}}_{M_t}(t_1) & \tilde{\mathcal{F}}_{M_t+1}(t_1)\\ \vdots & \vdots & \cdots & \vdots & \vdots\\ \tilde{\mathcal{F}}_1(t_{M_t}) & \tilde{\mathcal{F}}_2(t_{M_t}) & \cdots & \tilde{\mathcal{F}}_{M_t}(t_{M_t}) & \tilde{\mathcal{F}}_{M_t+1}(t_{M_t})\end{bmatrix}^T$$

and

$$\tilde{\mathcal{V}}_x=\begin{bmatrix}\tilde{\tilde{\mathcal{V}}}_1(x_0) & \tilde{\tilde{\mathcal{V}}}_2(x_0) & \cdots & \tilde{\tilde{\mathcal{V}}}_{M_t}(x_0) & \tilde{\tilde{\mathcal{V}}}_{M_x+1}(x_0)\\ \tilde{\tilde{\mathcal{V}}}_1(x_1) & \tilde{\tilde{\mathcal{V}}}_2(x_1) & \cdots & \tilde{\tilde{\mathcal{V}}}_{M_t}(x_1) & \tilde{\tilde{\mathcal{V}}}_{M_x+1}(x_1)\\ \vdots & \vdots & \cdots & \vdots & \vdots\\ \tilde{\mathcal{V}}_1(x_{M_x}) & \tilde{\mathcal{V}}_2(x_{M_x}) & \cdots & \tilde{\tilde{\mathcal{V}}}_{M_t}(x_{M_x}) & \tilde{\tilde{\mathcal{V}}}_{M_x+1}(x_{M_x})\end{bmatrix}^T.$$

To ensure a unique consistent solution for the STFPDEs, we must enforce the initial and boundary conditions. Within the spectral framework, these are treated as additional linear constraints on the unknown coefficient matrix $\mathcal{C}$. These conditions are defined as follows:

$$\left([\tilde{\mathcal{F}}_t]^{(1)}\otimes\tilde{\mathcal{V}}_x\right)\mathcal{C}=\mathcal{U}(x_i,0),\ i=0,1,2,\dots,M_x, \tag{3.8}$$

$$\left(\tilde{\mathcal{F}}_t \otimes \left[\tilde{\mathcal{V}}_x\right]^{(1)}\right)\mathcal{C} = \mathcal{U}(a, t_j),\ j = 0,1,2,\dots,M_t, \tag{3.9}$$

$$\left(\tilde{\mathcal{F}}_t \otimes \left[\tilde{\mathcal{V}}_x\right]^{(M_x+1)}\right)\mathcal{C} = \mathcal{U}(b, t_j),\ j = 0,1,2,\dots,M_t. \tag{3.10}$$

We determine the values of vector $\mathcal{C}$ by solving the system of Eqs (3.7)–(3.10). Thereafter, we use Eq (3.1) to obtain solutions for the STF Eq (1.1) or (1.2).

However, the current solution-set exhibits divergence. Consistent with our previous findings [11], convergence is achieved by normalizing the system vectors. To this end, we define the new orthonormal basis vectors as follows:

$$\Theta_x = \frac{\tilde{\mathcal{V}}_x}{\lambda_{x,0}},\ \Theta_x^{(1)} = \frac{\tilde{\mathcal{V}}_x^{(1)}}{\lambda_{x,1}},\ \Theta_x^{(2)} = \frac{\tilde{\mathcal{V}}_x^{(2)}}{\lambda_{x,2}},\ \Theta_t = \frac{\tilde{\mathcal{F}}_t}{\lambda_{t,0}}, \text{ and } \Theta_t^{(\alpha)} = \frac{\tilde{\mathcal{F}}_t^{(\alpha)}}{\lambda_{t,\alpha}}, \tag{3.11}$$

where $\lambda_{x,0} = \left\|\tilde{\mathcal{V}}_x\right\|_\infty$, $\lambda_{x,1} = \left\|\tilde{\mathcal{V}}_x^{(1)}\right\|_\infty$, $\lambda_{x,2} = \left\|\tilde{\mathcal{V}}_x^{(2)}\right\|_\infty$, $\lambda_{t,0} = \left\|\tilde{\mathcal{F}}_t\right\|_\infty$, and $\lambda_{t,\alpha} = \left\|\tilde{\mathcal{F}}_t^{(\alpha)}\right\|_\infty$.

Upon applying the orthonormal transformation to Eqs (3.7)–(3.10), the governing system is reformulated as follows:

$$\left[\left(\lambda_{t,\alpha}\left[\Theta_t^{(\alpha)}\right]^{(2:M_t+1)} \otimes [\Theta_x]^{(2:M_x)}\right)\mathcal{C}\right] + \rho\left[\left([\Theta_t]^{(2:M_t+1)} \otimes \lambda_{x,1}[\Theta_x]^{(2::M_x)}\right)\mathcal{C}\right] \circ \left[\left([\Theta_t]^{(2:M_t+1)} \otimes \left[\Theta_x^{(1)}\right]^{(2::M_x)}\right)\mathcal{C}\right]$$

$$-\varepsilon\left[\left([\Theta_t]^{(2:M_t+1)} \otimes \lambda_{x,2}\left[\Theta_x^{(2)}\right]^{(2::M_x)}\right)\mathcal{C}\right] + \sigma(\mathcal{N}_w) \circ \left[\left([\Theta_t]^{(2:M_t+1)} \otimes [\Theta_x]^{(2::M_x)}\right)\mathcal{C}\right] = [\underline{\mathbf{0}}], \tag{3.12}$$

$$\left(\Theta_t^{(1)} \otimes \Theta_x\right)\mathcal{C} = \mathcal{U}(x_i, 0),\ i = 0,1,2,\dots,M_x, \tag{3.13}$$

$$\left(\Theta_t \otimes \Theta_x^{(1)}\right)\mathcal{C} = \mathcal{U}(a, t_j),\ j = 0,1,2,\dots,M_t, \tag{3.14}$$

$$\left(\Theta_t \otimes \Theta_x^{(M_x+1)}\right)\mathcal{C} = \mathcal{U}(b, t_j),\ j = 0,1,2,\dots,M_t. \tag{3.15}$$

We determine the components of vector $\mathcal{C}$ by solving the system of Eqs (3.12)–(3.15). If the system is nonlinear (as in the case of STFBE), we implement the Newton-Raphson method. Conversely, if the system is linear (as in the case of STFHE), we solve it by the Inversion method. Thereafter, we use Eq (3.1) to get the proposed numerical solutions for the STF Eq (1.1) or (1.2).

While we described the spectral formulation based on SVFPs in the previous subsection, an alternative numerical strategy based on spline interpolation is presented next to provide another perspective for approximating the stochastic fractional models.

### *3.3. The spline interpolation approach for STFPDEs*

To facilitate the numerical solution of the STFPDEs using the TNPCS approach, the governing Eq (1.4) is discretized as follows:

$$[\mathcal{U}_{xx}]_i^j = \frac{1}{\varepsilon}\left(D_t^\alpha \mathcal{U}_i^j + \rho\mathcal{U}_i^j[\mathcal{U}_x]_i^j + \sigma\mathcal{U}_i^j n(t_j)\right). \tag{3.16}$$

For the fractional temporal domain, we apply the discretization of the fractional operator $D_t^{\alpha C}$ as defined in [30] as:

$$D_t^{\alpha C}\mathcal{U}_i^j = \frac{k^{-\alpha}}{\Gamma(2-\alpha)}\sum_{\tau=0}^{j-1}[((j-\tau)^{1-\alpha} - (j-\tau-1)^{1-\alpha})(\mathcal{U}_i^{\tau+1} - \mathcal{U}_i^\tau)]. \tag{3.17}$$

Additionally, we need to apply the finite difference method to approximate the derivatives for

$j = 0,1,2, \dots, M_t$:

$$(\mathcal{U}_x)_i^j = \left(\frac{1}{h_x}\right)\begin{cases}\mathcal{U}_{i+1}^j - \mathcal{U}_i^j, & i = 0,\\ \frac{1}{2}(\mathcal{U}_{i+1}^j - \mathcal{U}_{i-1}^j), & i = 1{:}\,M_x - 1,\\ \mathcal{U}_i^j - \mathcal{U}_{i-1}^j, & i = M_x,\end{cases}$$

and

$$n(t_j) = \frac{\varsigma}{k}\Big(\mathcal{B}(t_{j+1}) - \mathcal{B}(t_j)\Big). \tag{3.18}$$

Substituting these approximations into Eq (3.16) yields the following system:

$$[\mathcal{U}_{xx}]_i^j = \frac{k^{-\alpha}}{\varepsilon\Gamma(2-\alpha)}\sum_{\tau=0}^{j-1}[((j-\tau)^{1-\alpha} - (j-\tau-1)^{1-\alpha})(\mathcal{U}_i^{\tau+1} - \mathcal{U}_i^{\tau})]$$
$$+\frac{\rho}{\varepsilon}\mathcal{U}_i^j[\mathcal{U}_x]_i^j + \frac{\sigma\varsigma}{\varepsilon k}\Big(\mathcal{B}(t_{j+1}) - \mathcal{B}(t_j)\Big)\mathcal{U}_i^j, \tag{3.19}$$

By substituting the expressions from Eq (3.18) into Eq (2.19), the terms $[\mathcal{U}_{xx}]_i^j$, $[\mathcal{U}_{xx}]_{i-1}^j$, and $[\mathcal{U}_{xx}]_{i+1}^j$ are replaced to yield the proposed discrete system. This system is then solved for unknown coefficient matrix $\mathcal{C}$, subject to the specified initial and boundary conditions. For nonlinear systems (STFBE), the Newton–Raphson method is employed, whereas for linear systems (STFHE), the matrix inversion method is used to obtain the solutions for the STFPDEs (1.1) or (1.2).

In conclusion, the randomness inherent in the model equations, as evaluated via spectral and spline approaches, is tackled through a Monte Carlo simulation. In this context, several independent paths of the Brownian-motion process, referred to as $\mathcal{B}(t, \omega_k)$, are constructed, and the discretized equations are solved for each independent sample $\omega_k$, where the iteration is carried out for a finite number of times, $\mathcal{K}$. This process is followed by a statistical analysis, which includes the estimation of the mean and variance, offering a robust approach to the estimation of the approximate solutions of the STF Eq (1.1) or (1.2).

To provide a clear and structured overview of the two methodologies, here is a summarized breakdown of the functional steps for the spectral algorithm (SVFPs) and the spline algorithm (TNPCS):

**Dual spectral and spline algorithms:**

**Inputs:**

$\alpha$–fractional order,
$M_x$,$M_t$–grid sizes,
$a$,$b$,$T$–domain limits,
$x_i$,$t_j$–grid nodes,
$\mathcal{K}$–number of Monte-Carlo iterations,
$\rho$,$\varepsilon$,$\sigma$–SFPDE constants,
Initial and boundary conditions.

**Outputs:**

Mean trajectories,
Variance trajectories,
2D plots between required variables.

**Procedure:**

**Generate noise realizations:**

For each sample: $k = 1$ to $\mathcal{K}$,

Generate a realization of the Brownian motion process, $\mathcal{B}(t, \omega_k)$ over $t \in [0, T]$.

For

*Spectral approach:* compute the $\mathcal{B}(t)$ matrix and the $\mathcal{N}_w$ vector, Eqs (3.4) and (3.5).

*Spline approach:* compute increments: $\mathcal{B}(t_{k+1}) - \mathcal{B}(t_k)$ to get $n(t_k)$, Eq (3.18).

**Select the required approach:**

*Spectral approach:*

- Initialize SVFPs basis functions and their derivatives as defined in subsections 2.1 and 2.2.
- Compute the basis matrices: $\tilde{\mathcal{V}}_x$, $\tilde{\mathcal{V}}_x^{(1)}$, $\tilde{\mathcal{V}}_x^{(2)}$, $\tilde{\mathcal{F}}_t$, $\tilde{\mathcal{F}}_t^{(\alpha)}$, $P(x_i)$, and $Q(t_j)$, Eqs (3.6) and (3.7).
- Normalize the basis matrices: $\Theta_x$, $\Theta_x^{(1)}$, $\Theta_x^{(2)}$, $\Theta_t$, and $\Theta_t^{(\alpha)}$, Eq (3.11).
- For $k = 1$ to $\mathcal{K}$ (Noise samples loop).

Set the vector of unknown spectral coefficients, $\mathcal{V}$.

Construct the governing system using Kronecker products of the basis function and their derivative submatrices for all grid points, Eqs (3.12)–(3.15).

Solve this system to get the vector, $\mathcal{V}$.

Then, compute the full solution using Eq (3.1).

Store the current solution and repeat for the next $k$.

End for loop.

- Collect full trajectory for ensemble $k$.

*Spline approach:*

- Initialize the TNPCS basis function as defined in subsection 2.3.
- Apply the discretization of the fractional derivative $D_t^{\alpha C}$, Eq (3.7).
- Apply the finite difference method to approximate $\mathcal{U}_x$ and noise $n(t)$, Eq (3.19).
- For $k = 1$ to $\mathcal{K}$ (noise samples loop).

For $j = 1$ to $M_t$ (time level loop).

Define the current $n(t_j)$.

Compute $[\mathcal{U}_{xx}]_i^j$ using Eq (3.17). Then use it to define $[\mathcal{U}_{xx}]_{i-1}^j$ and $[\mathcal{U}_{xx}]_{i+1}^j$.

Substitute the expressions into Eq (2.18).

Solve the system for the current level and repeat for the next $j$.

End time level loop.

- Store the current solution and repeat for the next $k$.

End noise samples loop.

- Collect full trajectory for ensemble $k$.

**Statistical aggregation:**

- Collect solutions across all noise samples: $\mathcal{U}^{(k)} = \{\mathcal{U}_{i,j}^1, \mathcal{U}_{i,j}^2, \mathcal{U}_{i,j}^3, \dots, \mathcal{U}_{i,j}^{\mathcal{K}}\}$.
- Determine the variance and mean for each ensemble:

$$\mathcal{U}_{mean} = \frac{1}{\mathcal{K}} \sum_{k=1}^{\mathcal{K}} \mathcal{U}^{(k)},$$

$$\mathcal{U}_{var} = \frac{1}{\mathcal{K}-1} \sum_{k=1}^{\mathcal{K}} \left(\mathcal{U}^{(k)} - \mathcal{U}_{mean}\right)^2.$$

**Visualization:**

- Generate 3D Plots for mean and variance.
- Generate 2D plots between selected mean and variance trajectories for different fractional order $\alpha$ or noise amplitude $\sigma$.

## 4. Results

After establishing the numerical formulations of the proposed approaches, we evaluate their performance through several computational experiments. In this following section, we present numerical results obtained from representative stochastic fractional models.

The computation is done by setting the temporal step equal to $0.05$, varying the spatial steps, and averaging the result of 2,000 independent stochastic realizations. The result shows the structural stability of the mean profile even after being affected by stochastic elements. The underlying geometry of the solution is not affected in any way, even when considering the effects of additive white noise. It follows, therefore, that the methods can filter out the stochastic elements to reveal the underlying deterministic behavior of the system, showing that the expectation tends to converge.

**Problem 1.** Consider the STF Burger's equation [20]:

$$\mathcal{U}_{xx}(x,t) = D_t^{\alpha}\mathcal{U}(x,t) + \mathcal{U}(x,t)\,\mathcal{U}_x(x,t) + \sigma\mathcal{U}(x,t)n(t),$$

$$\mathcal{U}(x,0) = 1 - \frac{1}{2}\sin^2 x,\ \ t \in [0,1],$$

Following the absence of explicit boundary conditions in [20], we employ the Adomian Decomposition Method to derive an analytical approximation for them. By evaluating the decomposition series at$x = \pm\pi$ based on the initial condition, we obtain the following approximation:

$$\mathcal{U}(-\pi,t) = \mathcal{U}(\pi,t) \cong 1 + \frac{t^{\alpha}}{\Gamma(\alpha+1)} + \frac{3t^{2\alpha}}{\Gamma(2\alpha+1)} - \left(6 + \frac{\Gamma(2\alpha+1)}{\Gamma(\alpha+1)^2}\right)\frac{t^{3\alpha}}{\Gamma(3\alpha+1)},\ \ x \in [-\pi,\pi].$$

**Problem 2.** For the STF heat equation [21]:

$$D_t^{\alpha}\mathcal{U}(x,t) = \mathcal{U}_{xx}(x,t) + \sigma\mathcal{U}(x,t)n(t),$$

$$\mathcal{U}(x,0) = \sin x,\ \ t \in [0,1],$$

$$\mathcal{U}(0,t) = \mathcal{U}(\pi,t) = 0,\ \ x \in [0,\pi].$$

The numerical outcomes for Problem 1, computed with the help of the proposed SVFPs and TNPCS methods, are summarized and presented in Table 1. Moreover, a comparative error analysis, as provided in Table 2, may be conducted to validate the results and accuracy of the SVFPs method. For the purpose of carrying out the error analysis, the calculation of the errors using the proposed method of SVFPs is carried out using a temporal step size of $0.1$, while the results computed by the Galerkin finite element (Galerkin FE) method [21] are obtained using a much higher temporal resolution of $2^{-10}$.

The accuracy is quantified in terms of the $L_2$ norm error, as defined in [21]:

$$E\|e^j\|_2 = \|\mathcal{U}_h^j - \mathcal{U}(t_j)\|_2,$$

where $\mathcal{U}(t_j)$ denotes the expectation of solutions, $\mathcal{U}_h^j$ denotes the numerical solution with a space step $h$ and a time level of $t_j$, and the expected-values $E\|.\|$ are estimated by taking an average over one hundred independent stochastic values according to benchmarks provided in [21].

The computational result of the SVFPs method also delivers a high degree of accuracy with a larger temporal step, as shown in Table 1, compared to the Galerkin FE method. This indicates the computational efficiency and the better convergence of the spectral technique in the dynamics of stochastic fractional domains.

**Table 1.** The approximate solutions for Problem 1 for $\sigma = 0.25$ and $t = 1$.

| $x$ | SVFPs | | TNPCS | |
|---|---|---|---|---|
| | $\alpha$=0.7 | $\alpha$=0.9 | $\alpha$=0.7 | $\alpha$=0.9 |
| $-3\pi/4$ | 0.608200 | 0.543351 | 0.505741 | 0.500771 |
| $-\pi/2$ | 0.431957 | 0.394621 | 0.568752 | 0.595828 |
| $-\pi/4$ | 0.632663 | 0.554246 | 0.615047 | 0.595828 |
| 0 | 0.831898 | 0.713986 | 0.785381 | 0.605721 |
| $\pi/4$ | 0.632664 | 0.554246 | 0.862217 | 0.778211 |
| $\pi/2$ | 0.431967 | 0.394621 | 0.703404 | 0.895243 |
| $3\pi/4$ | 0.608027 | 0.543358 | 0.668901 | 0.706192 |

**Table 2.** The $L_2$ norm error of Problem 2 in the spatial direction for $x \in [0, 2]$.

| $\alpha$ | $M_x$ | $E\|e^j\|_2$ by SVFPs | $E\|e^j\|_2$ by Galerkin FE [21] |
|---|---|---|---|
| 0.55 | 10 | $3.3271\times10^{-5}$ | $3.4531\times10^{-2}$ |
| | 20 | $1.5404\times10^{-5}$ | $2.3785\times10^{-3}$ |
| | 40 | $3.1843\times10^{-6}$ | $1.5930\times10^{-4}$ |
| | 80 | $7.7976\times10^{-7}$ | $1.1049\times10^{-5}$ |
| 0.7 | 10 | $7.5277\times10^{-5}$ | $3.4135\times10^{-2}$ |
| | 20 | $1.5667\times10^{-5}$ | $2.3350\times10^{-3}$ |
| | 40 | $3.7576\times10^{-6}$ | $1.5530\times10^{-4}$ |
| | 80 | $2.0807\times10^{-6}$ | $1.0477\times10^{-5}$ |
| 0.9 | 10 | $3.0546\times10^{-6}$ | $3.3997\times10^{-2}$ |
| | 20 | $1.9856\times10^{-6}$ | $2.3096\times10^{-3}$ |
| | 40 | $1.5336\times10^{-6}$ | $1.5467\times10^{-4}$ |
| | 80 | $5.8325\times10^{-7}$ | $1.1001\times10^{-5}$ |

Figures 1, 2, 4, and 5 show the statistical mean of the numerical solution in 2D and 3D for Problems 1 and 2 with a range of fractional orders and noise amplitudes $\alpha$ and $\sigma$, respectively. These examples intend to convey how the mean is affected by varying levels of order, as well as display the structural stability of the mean profile with respect to stochastic influence. Additionally, Figures 3 and 6 depict the variance of the numerical results concerning the analysis of the problems with different $\alpha$ and $\sigma$. These figures help us carry out a rigorous comparative analysis between the proposed SVFPs method and the TNPCS method.

The outcome of these calculations illustrates exceptionally high-resolution nodal accuracy of the SVFPs-based strategy, along with strict computational stability and boundedness within high-intensity noise regimes, substantially reducing the numerical instability that generally accompanies high levels of stochastic excitation. This indicates that the spectral-based methodology is well-suited to handling the long-memory effects of fractional operators without falling into the phenomenon of stochastic volatility.

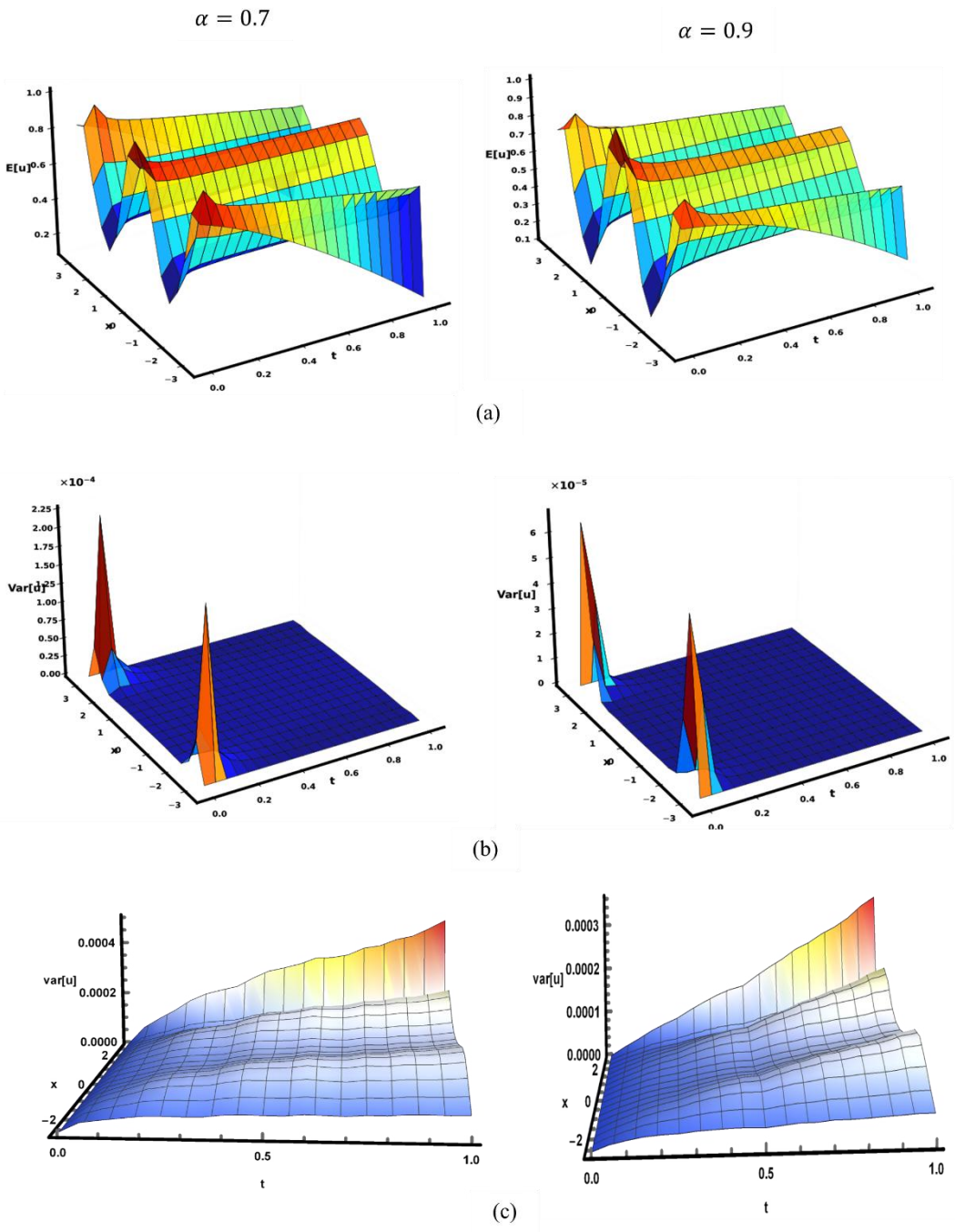


**Figure 1.** Spatial profile of the mean field and variance field for the solution of the STF Burger's equation (Problem 1), with stochastic forcing intensity $\sigma = 0.25$: (a) Mean field, and the variance field given by (b) SVFPs and (c) TNPCS.

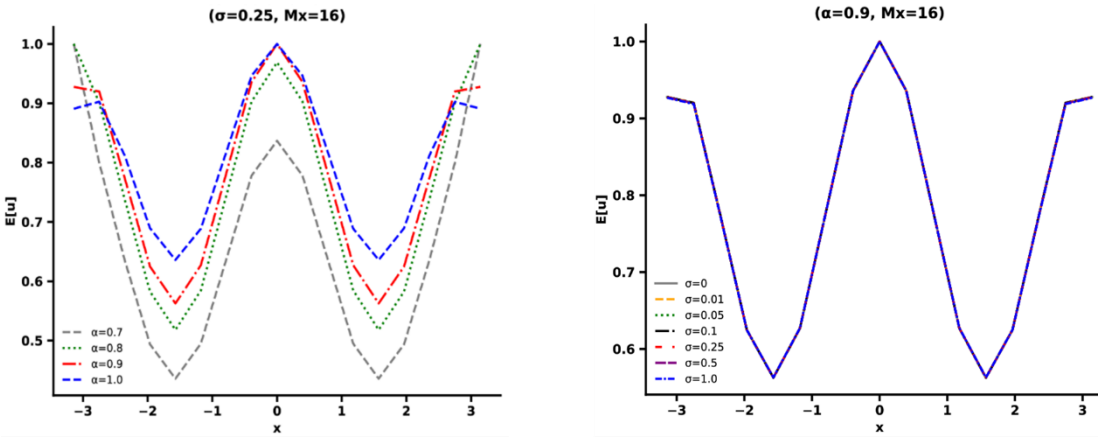


**Figure 2.** Spatial profile of the mean field for the solution of the STF Burger's equation (Problem 1), across fractional orders $\alpha$ and noise amplitudes $\sigma$, and $t = 1$.

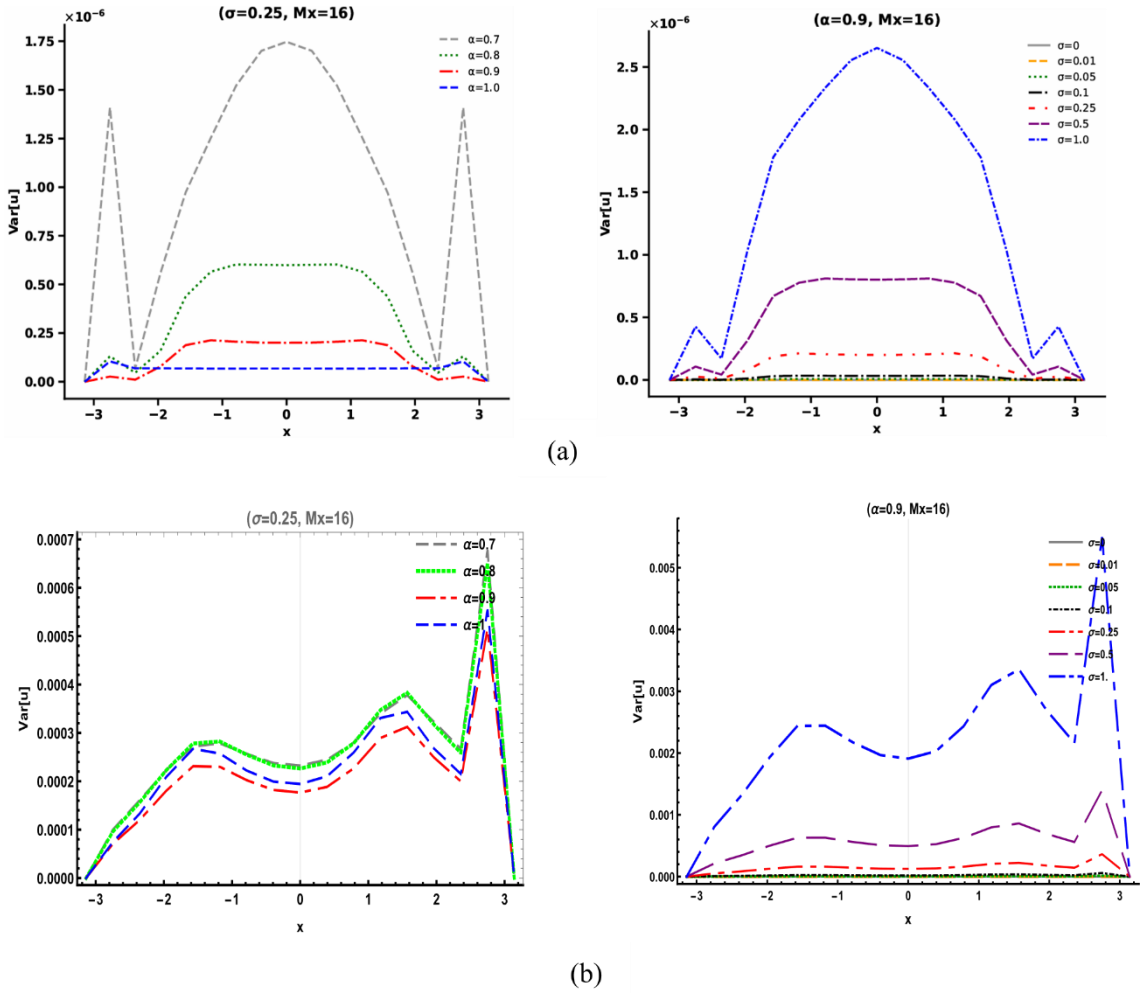


**Figure 3.** Spatial profile of the variance field for the solution of the STF Burger's equation (Problem 1), across fractional orders $\alpha$ and noise amplitudes $\sigma$ by: (a) SVFPs and (b) TNPCS.

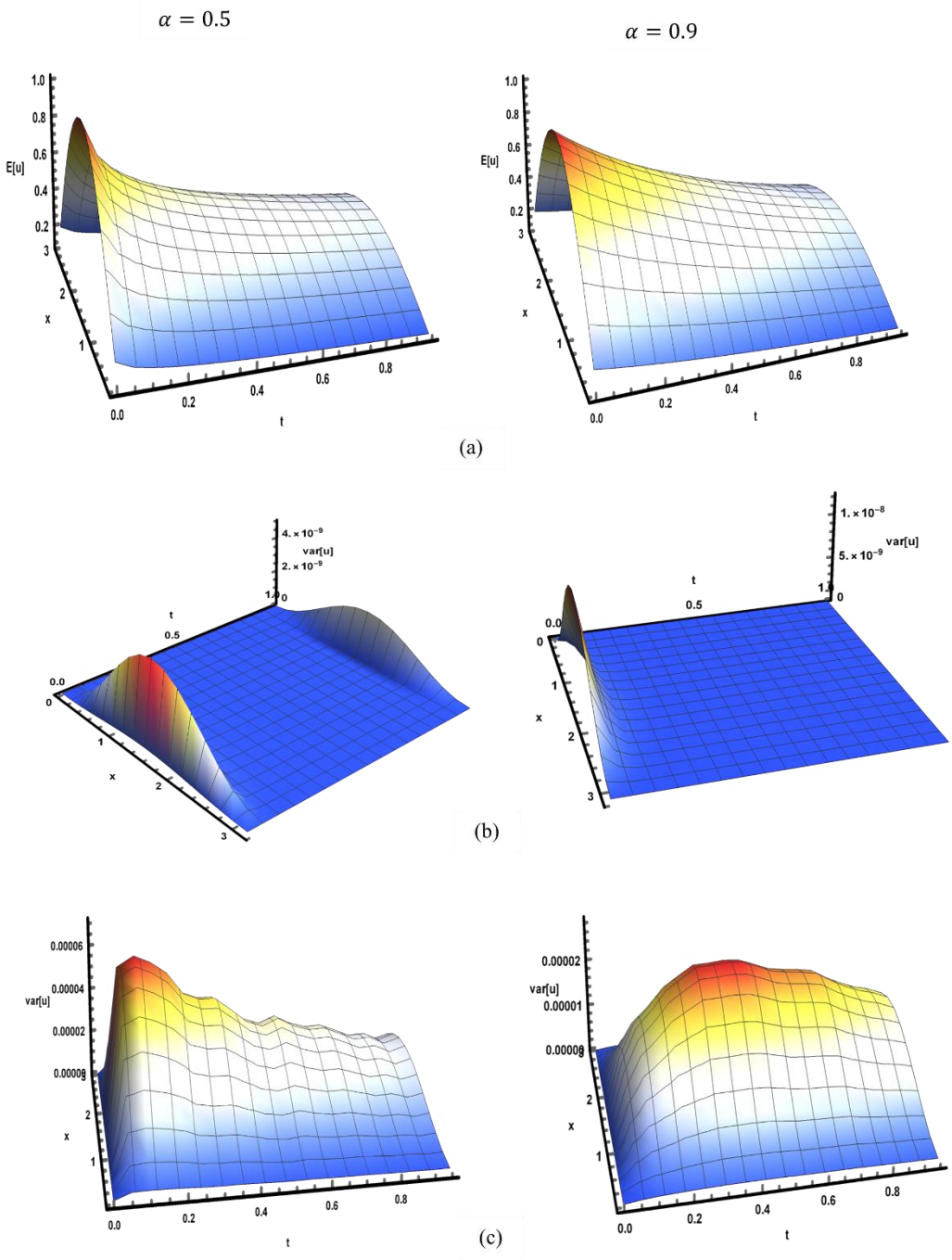


**Figure 4.** Spatial profile of the mean field and variance field for the solution of the STF heat equation (Problem 2), with stochastic forcing intensity $\sigma = 0.25$: (a) Mean field, and the variance field given by (b) SVFPs and (c) TNPCS.

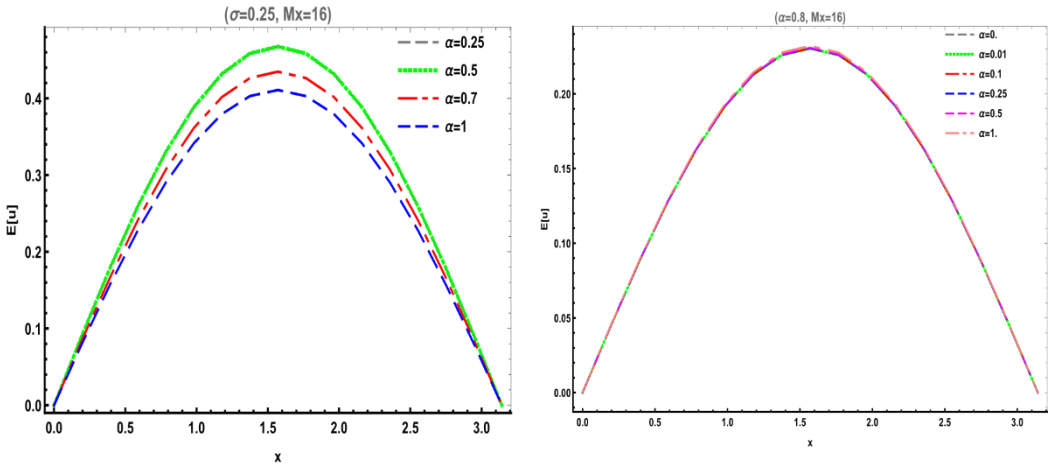


**Figure 5.** Spatial profile of the mean field for the solution of the STF heat equation (Problem 2), across fractional orders $\alpha$ and noise amplitudes $\sigma$, and $t = 1$.

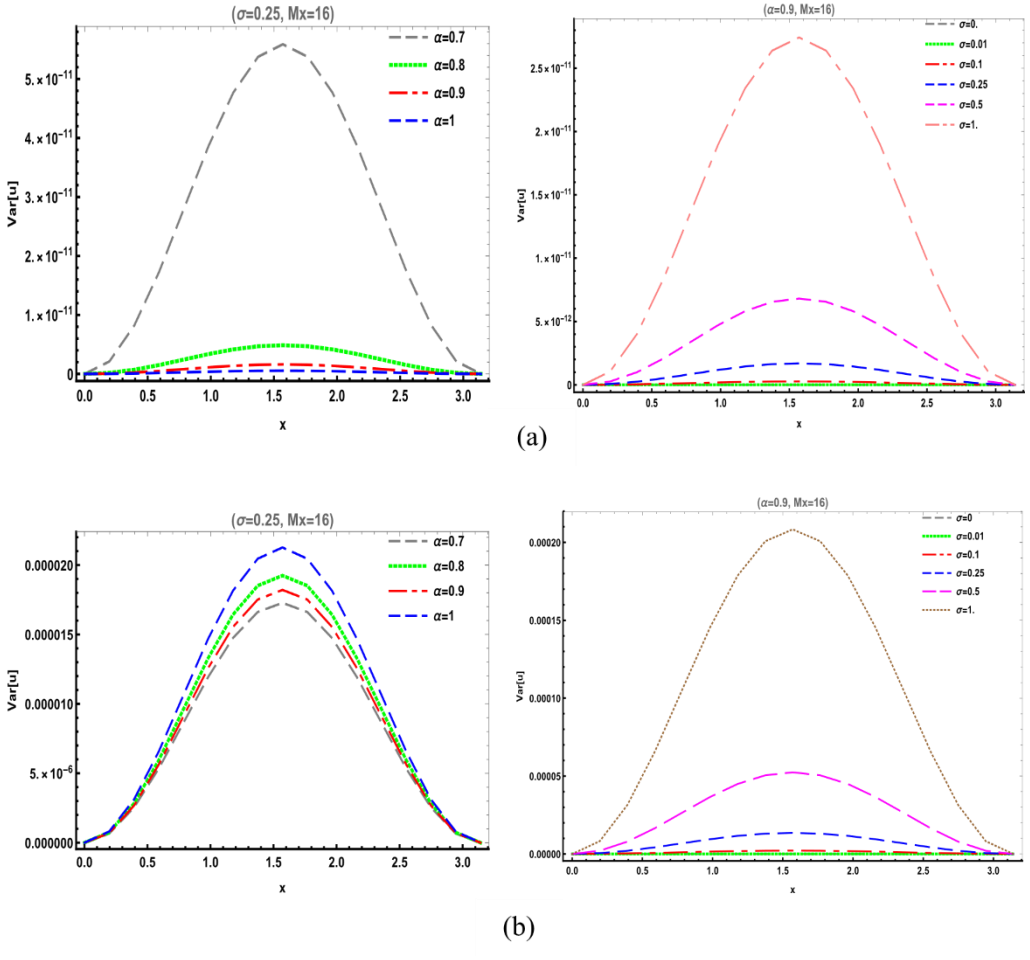


**Figure 6.** Spatial profile of the variance field for the solution of the STF heat equation (Problem 2), across fractional orders $\alpha$ and noise amplitudes $\sigma$ by: (a) SVFPs and (b) TNPCS.

To ensure a fair comparison with numerical techniques, the Galerkin FE method reported in [21] is implemented following the same spatial domain and boundary conditions used in this study. The spatial interval $x \in [0,2]$ is divided into $M_x$ uniform elements, and piecewise linear basis functions are used to construct the FE approximation space.

For temporal discretization, the same time step size $k$ is employed both the FE method and the proposed schemes to maintain consistency in the comparison. The resulting system of algebraic equations obtained from the Galerkin formulation is solved using standard matrix assembly procedures and iterative solvers. The stochastic forcing term is generated using identical realizations of the white noise process for all methods to ensure that the numerical results are evaluated under comparable stochastic conditions.

These implementation settings enable the comparison presented in Table 2 to reflect the intrinsic accuracy of the numerical schemes rather than differences in discretization parameters.

One important observation from Table 2 is that the SVFPs method keeps high accuracy even for relatively coarse spatial resolutions. This attitude can be attributed to the spectral nature of the SVFP approximation. Unlike local discretization techniques such as finite differences or low-order finite element methods, the SVFP approach represents the solution using a set of global basis functions derived from sifted Vieta–Fibonacci polynomials.

Because these basis functions capture the global structure of the solution, the approximation error decreases rapidly as the number of modes increases. Furthermore, the fractional derivative introduces memory effects that extend over the temporal interval. The spectral representation used in the SVFP formulation is particularly effective in approximating such nonlocal operators, which contributes to the improved numerical accuracy observed in the experiments.

Another important factor is the stability of the spectral expansion. The SVFP basis distributes numerical errors across the computational domain rather than concentrating them locally, which helps maintain stability even when relatively large time steps are used.

In addition to the comparison with the Galerkin FE method, the accuracy behavior shown in Table 2 is consistent with results reported in other studies on stochastic fractional equations using finite difference and spline-based schemes. In particular, many local discretization methods require significantly finer meshes to achieve similar accuracy levels due to the presence of fractional memory terms and stochastic perturbations.

The results obtained in this study indicate that the proposed SVFPs and TNPCS schemes provide competitive accuracy while maintaining computational efficiency. These findings support the potential of spectral-spline frameworks as effective tools for solving stochastic fractional models.

The numerical experiments presented above demonstrate the effectiveness of the presented approaches in approximating stochastic fractional dynamics. Based on these findings, the major findings and implications of the study are summarized in the following conclusion section.

## 5. Conclusions

In this study, we presented a thorough numerical investigation into the solution of STFPDEs via two methodologies, SVFPs and TNPCS. Further, these two methods have been independently applied to STF Burger's and STF heat equations to test the individual performance of these methods in elucidating the interaction between fractional memory and stochastic variability.

Our comparative analysis shows that both schemes provide high-precision approximations in terms of white noise perturbations. The numerical results demonstrate that both schemes of the SVFPs and TNPCS methods perform superiorly to existing state-of-the-art results in literature. The critical

observation, however, is the solution variance with respect to the level of noise amplitude $\sigma$, as well as the fractional order $\alpha$:

- *Boundedness:* While the strength of the noise grows, the variance is strictly bounded. This is a remarkable property, as it prevents any numerical "blow-up" problems, which are common in standard finite difference schemes when subjected to strong stochastic driving.
- *Methodological contrast:* Although both methods have shown good robustness, the accuracy of SVFPs is better compared to the rest when it comes to high-resolution accuracy. This is due to its ability to maintain computational stability via its spectral basis, which distributes the noise energy throughout a specified domain.
- *Stochastic resilience:* The consistency in the variance profile within a large range of values of $\sigma$ and $\alpha$ assures the credibility of the presented schemes. This strength is vital if we consider real-world systems characterized by stochastic volatility.

Moreover, this work provides a flexible computational platform, as it can offer researchers two viable routes for ongoing attempts to model anomalous diffusion and hereditary processes in complex stochastic environments. Although the current implementation is intended for the analysis of one-dimensional benchmarks, the logic of the two platforms of SVFPs and TNPCS is intrinsically scalable in nature. As such, the extension of this line of research might potentially include the extension of this methodology toward multi-dimensional spaces, especially in the presence of multiplicative noise or Fractional-Gaussian fluctuations.

## Author contributions

Aisha F. Fareed: formal analysis, investigation, literature review, writing review, and editing; Mourad S. Semary: mathematical analysis, validation, formal analysis, and editing; Dokhyl M. Alqahtani: investigation, and formal analysis; Emad A. Mohamed: investigation and validation; Ahmed G. Khattab: conceptualization, investigation, validation, mathematical analysis, writing the original draft, and formal analysis. All authors have read and agreed to the published version of the manuscript.

## Use of Generative-AI tools declaration

The authors declare they have not used artificial intelligence (AI) tools in the creation of this article.

## Acknowledgments

This study is supported via funding from Prince Sattam bin Abdulaziz University project number (PSAU/2026/R/1447).

## Conflicts of interest

The authors declare no conflicts of interest in this paper.

## References


1 F. Liu, P. Zhuang, Q. Liu, *Numerical methods of fractional partial differential equations and applications*, Science Press, 2015.

2 D. Baleanu, K. Diethelm, E. Scalas, J. J. Trujillo, *Fractional calculus: models and numerical methods*, World Scientific, 2012. https://doi.org/10.1142/8180

3 M. D'Elia, Q. Du, C. Glusa, M. Gunzburger, X. Tian, Z. Zhou, Numerical methods for nonlocal and fractional models, *Acta Numer.*, **29** (2020), 1–124. https://doi.org/10.1017/S096249292000001X

4 R. L. Magin, Fractional calculus models of complex dynamics in biological tissues, *Comput. Math. Appl.*, **59** (2010), 1586–1593. https://doi.org/10.1016/j.camwa.2009.08.039

5 K. Moaddy, A. G. Radwan, K. N. Salama, S. Momani, I. Hashim, The fractional-order modeling and synchronization of electrically coupled neuron systems, *Comput. Math. Appl.*, **64** (2012), 3329–3339. https://doi.org/10.1016/j.camwa.2012.01.005

6 A. Kilbas, H. M. Srivastava, J. J. Trujillo, *Theory and applications of fractional differential equations*, Elsevier, 2006.

7 A. F. Fareed, M. S. Semary, Stochastic improved Simpson for solving nonlinear fractional-order systems using product integration rules, *Nonlinear Eng.*, **14** (2025), 20240070. https://doi.org/10.1515/nleng-2024-0070

8 A. F. Fareed, E. A. Mohamed, A. Mokhtar, M. S. Semary, A novel fractional integral transform-based homotopy perturbation method for some nonlinear differential systems, *Fractal Fract.*, **9** (2025), 212. https://doi.org/10.3390/fractalfract9040212

9 D. Uma, H. Jafari, S. R. Balachandar, S. G. Venkatesh, An approximation method for stochastic heat equation driven by white noise, *Int. J. Appl. Comput. Math.*, **8** (2022), 274. https://doi.org/10.1007/s40819-022-01376-4

10 A. Nouy, Recent developments in spectral stochastic methods for the numerical solution of stochastic partial differential equations, *Arch. Comput. Methods Eng.*, **16** (2009), 251–285. https://doi.org/10.1007/s11831-009-9034-5

11 A. G. Khattab, D. A. Hammad, M. S. Semary, E. A. Mohamed, I. Malik, A. F. Fareed, A novel spectral framework for stochastic differential equations: leveraging shifted Vieta-Fibonacci polynomials, *AIMS Math.*, **10** (2025), 30134–30161. https://doi.org/10.3934/math.20251324

12 A. F. Fareed, A. G. Khattab, M. S. Semary, A novel stochastic ten non-polynomial cubic splines method for heat equations with noise term, *Partial Differ. Equations Appl. Math.*, **10** (2024) 100677. https://doi.org/10.1016/j.padiff.2024.100677

13 Y. H. Youssri, M. M. Muttardi, A mingled tau-finite difference method for stochastic first-order partial differential equations, *Int. J. Appl. Comput. Math.*, **9** (2023), 14. https://doi.org/10.1007/s40819-023-01489-4

14 M. Gerencsér, I. Gyöngy, Finite difference schemes for stochastic partial differential equations in Sobolev spaces, *Appl. Math. Optim.*, **72** (2015), 77–100. https://doi.org/10.1007/s00245-014-9272-2

15 A. G. Khattab, M. S. Semary, D. A. Hammad, A. F. Fareed, Exploring stochastic heat equations: a numerical analysis with fast discrete fourier transform techniques, *Axioms*, **13** (2024), 886. https://doi.org/10.3390/axioms13120886

16 I. Masti, K. Sayevand, On collocation-Galerkin method and fractional B-spline functions for a class of stochastic fractional integro-differential equations, *Math. Comput. Simul.*, **216** (2024), 263–287. https://doi.org/10.1016/j.matcom.2023.09.013

17 A. F. Fareed, E. A. Mohamed, M. Aly, M. S. Semary, A novel numerical method for stochastic conformable fractional differential systems, *AIMS Math.*, **10** (2025) 7509–7525. https://doi.org/10.3934/math.2025345

18 A. F. Fareed, M. Aly, E. A. Mohamed, M. S. Semary, An effective numerical approach to stochastic systems with conformable fractional noise: a unified analysis of convergence and stability, *Mathematics*, **13** (2025), 3966. https://doi.org/10.3390/math13243966

19 R. Anton, D. Cohen, L. Quer-Sardanyons, A fully discrete approximation of the one-dimensional stochastic heat equation, *IMA J. Numer. Anal.*, **40** (2020), 247–284. https://doi.org/10.1093/imanum/dry060

20 S. M. Hosseini, Z. Asgari, Solution of stochastic nonlinear time fractional PDEs using polynomial chaos expansion combined with an exponential integrator, *Comput. Math. Appl.*, **73** (2017), 997–1007. https://doi.org/10.1016/j.camwa.2016.07.021

21 G. A. Zou, A Galerkin finite element method for time-fractional stochastic heat equation, *Comput. Math. Appl.*, **75** (2018), 4135–4150. https://doi.org/10.1016/j.camwa.2018.03.019

22 R. Sharma, Rajeev, A numerical approach based on Vieta–Fibonacci polynomials to solve fractional order advection–reaction diffusion problem, *J. Anal.*, **33** (2024), 1251–1275. https://doi.org/10.1007/s41478-024-00804-6

23 A. Moumen, A. Mennouni, M. Bouye, A novel Vieta–Fibonacci projection method for solving a system of fractional integrodifferential equations, *Mathematics*, **11** (2023), 3985. https://doi.org/10.3390/math11183985

24 S. M. Sivalingam, P. Kumar, V. Govindaraj, R. A. Qahiti, W. Hamali, Z. M. Mutum, An operational matrix approach with Vieta-Fibonacci polynomial for solving generalized Caputo fractal-fractional differential equations, *Ain Shams Eng. J.*, **15** (2024), 102678. https://doi.org/10.1016/j.asej.2024.102678

25 H. Azin, M. H. Heydari, F. Mohammadi, Vieta–Fibonacci wavelets: application in solving fractional pantograph equations, *Math. Methods Appl. Sci.*, **45** (2022), 411–422. https://doi.org/10.1002/mma.7783

26 K. Sadri, K. Hosseini, D. Baleanu, S. Salahshour, C. Park, Designing a matrix collocation method for fractional delay integro-differential equations with weakly singular kernels based on Vieta–Fibonacci polynomials, *Fractal Fract.*, **6** (2022), 2. https://doi.org/10.3390/fractalfract6010002

27 P. Agarwal, A. A. El-Sayed, J. Tariboon, Vieta–Fibonacci operational matrices for spectral solutions of variable-order fractional integro-differential equations, *J. Comput. Appl. Math.*, **382** (2021), 113063. https://doi.org/10.1016/j.cam.2020.113063

28 M. H. Heydari, Z. Avazzadeh, A. Atangana, Shifted Vieta-Fibonacci polynomials for the fractal-fractional fifth-order KdV equation, *Math. Methods Appl. Sci.*, **44** (2021), 7219. https://doi.org/10.1002/mma.7219

29 D. A. Hammad, M. S. Semary, A. G. Khattab, Ten non-polynomial cubic splines for some classes of Fredholm integral equations, *Ain Shams Eng. J.*, **13** (2022), 101666. https://doi.org/10.1016/j.asej.2021.101666

30 D. A. Hammad, M. S. Semary, A. G. Khattab, Parametric quintic spline for time fractional Burger's and coupled Burgers' equations, *Fixed Point Theory Algorithms Sci. Eng.*, **2023** (2023), 9. https://doi.org/10.1186/s13663-023-00740-3



AIMS Press